Article:
Maybee, B. orcid.org/0000-0001-7834-9489, Bassford, J., Marsham, J. et al. (4 more authors) (Accepted: 2025) How sensitive are Sahelian Mesoscale Convective Systems to cold pool suppression? Quarterly Journal of the Royal Meteorological Society. ISSN 0035-9009 (In Press)

https://doi.org/10.1002/qj.5032

ORIGINAL ARTICLE

Journal Section

How sensitive are Sahelian Mesoscale Convective Systems to cold pool suppression?

Ben Maybee[1] | James Bassford[1] | John H. Marsham[1] | Huw Lewis[2] | Paul Field[2] | Cornelia Klein[3] | Douglas J. Parker[1,4,5]

[1]School of Earth and Environment, University of Leeds, Leeds, UK

[2]Met Office, Exeter, UK

[3]UK Centre for Ecology and Hydrology (UKCEH), Wallingford, United Kingdom

[4]National Centre for Atmospheric Science (NCAS), University of Leeds, Leeds, UK

[5]NORCE Norwegian Research Centre AS, Bjerknes Center for Climate Research, Bergen, Norway

Correspondence
Ben Maybee, School of Earth and Environment, University of Leeds, Leeds, UK
Email: b.w.maybee@leeds.ac.uk

Funding information
NERC grant LMCS, NE/W001888/1. NERC independent research fellowship COCOON, NE/X017419/1

Understanding the physical processes driving deep convective storms is an essential prerequisite for understanding the wider tropical atmosphere. Cold pools driven by rainfall evaporation are a ubiquitous feature of Mesoscale Convective Systems (MCSs) that have especially pronounced upscale effects in the climate of the West African Sahel, through their modulation of the regional monsoon circulation. The role of cold pools in determining the dynamics, lifecycle and propagation of tropical MCSs themselves, however, remains debated. Here we probe the feedback of cold pools on Sahelian MCS characteristics through a 40 day, 2.2 km convection-permitting Met Office Unified Model sensitivity experiment in which rainfall evaporation is switched off in the microphysics scheme. Storms generated in the sensitivity experiment subsequently show strongly suppressed cold pool density currents versus a Control simulation. Yet we find no statistically significant difference between the diurnal cycles of MCS counts, with continued nocturnal propagation of storms in the experiment, and a reduction of MCS speeds by 1.7 ms^{-1} caused by a similar slow–down in the African Easterly Jet due to a weak-

Abbreviations: MCS, Mesoscale Convective System; CP, convection–permitting; AEJ, African Easterly Jet; BT, brightness temperature; LNB, level of neutral buoyancy; MSE, Moist Static Energy; CAPE, Convective Available Potential Energy

ened large-scale meridional temperature gradient. Indeed, the main differences between the simulations are in the regional mean state and diurnal cycles of MCS rainfall. Changes to composite updraft geometry are consistent with the role of cold pool horizontal vorticity in balancing the strong low-level wind shear characteristic of the region. Remarkably though, we find no sensitivity of the positive scaling of MCS rainfall with shear to cold pools, with reduced entrainment-dilution under stronger shear conditions the fundamental physics driving the relationship. Our results help to disentangle processes in the Sahel in which cold pools play a driving role (nocturnal rainfall intensification, regional circulation) from those in which they are passive actors, which we find primarily to be MCS development, propagation, and rainfall-shear scalings.

KEYWORDS
Cold pools, MCSs, West African Sahel, wind shear, convection–permitting modelling

1 | INTRODUCTION

It is frequently stated that convective cold pools play an essential role in the dynamics of Mesoscale Convective Systems (MCSs). MCSs are an archetypal form of convective organisation, comprising clusters of thunderstorms which merge to form large, cold anvil clouds. Their structure is complex and comprised of features spanning a wide range of scales from high, cold anvil shields spanning 1000's of square kilometres, to sub–kilometre entrainment and microphysical processes (Houze Jr (2004)). Evaporation of rainfall from multiple embedded kilometre–scale convective updrafts leads to cooling of ambient air and the formation of downdrafts: this cool, negatively buoyant air sinks, forming convective cold pools at the MCS base. These form multiple propagating density currents which can merge to form large, organised systems with rich structures (Drager and van den Heever (2017); Fuglestvedt and Haerter (2020)).

Cold pools are one of MCSs' most striking observed features, typically causing significant decreases in surface temperature, increases in surface pressure, strong winds and an increase in relative humidity as the ambient surface layer is displaced by their cool, dense air (Engerer et al. (2008); Provod et al. (2016)). They are features common to all flavours of convective rainfall, and an integral component of convective organisation across scales (Tompkins (2001); Bony et al. (2015)). Gust fronts at cold pool boundaries enable the triggering of new convective cells through both moisture convergence and mechanical lifting (Torri et al. (2015)), with cold pool collisions enhancing this effect (Meyer and Haerter (2020); Fuglestvedt and Haerter (2020)). Idealised large–eddy simulations, typically using experiments where rainfall evaporation is turned off and cold pools inhibited, show that cold pools play a critical role in the transition from shallow to deep convection (Khairoutdinov and Randall (2006)), but that their impact on organisation is a non-linear function of domain size (Jeevanjee and Romps (2013)).

In mature MCSs, cold pools are canonically understood to maintain mature storms and determine their updraft geometry (Rotunno et al. (1988), RKW hereafter) by providing a balance to the horizontal vorticity generated by low–level vertical wind shear. Predictions derived from such arguments for the speeds, shear–relative orientation and updraft tilts of midlatitude MCSs are well verified by numerical experiments (Robe and Emanuel (2001); Weisman and Rotunno (2004); Bryan et al. (2006); Abramian et al. (2022)). However, experiments again turning off rainfall evaporation in both idealised and realistic model setups have shown repeatedly that MCSs can continue to initiate, mature and propagate without cold pools (Crook and Moncrieff (1988); Stoelinga et al. (2003); Schumacher (2009); Trier et al. (2011); Clark et al. (2014); Grant et al. (2018, 2020)). Moreover, MCS rainfall in observed storms increases under stronger environmental shear (Senior et al. (2021); Chen et al. (2023); Hsiao et al. (2024)). This positive feedback can be explained without reference to cold pools, through shear modulation of low–level unstable inflow (Alfaro (2017); Bickle et al. (2021)) causing a decrease in updraft entrainment rates at higher shear found in both idealised experiments (Mulholland et al. (2021); Abramian et al. (2023)) and regional simulations with explicit convection (Maybee et al. (2024)).

Questions surrounding the role of cold pools in MCS dynamics are of great practical importance in the semi–arid Sahel region of West Africa, some parts of which receive over 90% of their seasonal rainfall totals from the long–lived propagating MCSs (Mathon et al. (2002)) supported by strong wind shear between the low–level monsoon flow and mid–level African Easterly Jet (AEJ) (Parker and Diop-Kane (2017)). These MCSs form huge, country–scale cold pools (Provod et al. (2016); Hoeller et al. (2024)), generating cool, moist outflows into the Sahara which mediate the northerly propagation of the West African monsoon (Marsham et al. (2013); Birch et al. (2014a); Trzeciak et al. (2017)). Convective cold pool misrepresentation in models leads to significant biases both in Saharan temperatures and dust transport (Marsham et al. (2011); Garcia-Carreras et al. (2013, 2021)). Wind shear exercises important controls on MCSs in this region, with stronger shear due to a strengthening meridional temperature gradient responsible for an observed intensification in extreme MCS rainfall (Taylor et al. (2017)). Global climate models underpinning projections of future Sahel rainfall do not resolve this mechanism, with projections of extremes significantly increased when combined with observed MCS rainfall–shear scalings (Klein et al. (2021)). While thermodynamic drivers naturally provide the leading control on projected trends in the regions' MCSs (Bickle et al. (2021); Zhao et al. (2024)), the physics of MCS–shear interactions, and thus cold pools, is a crucial component of improving climate projections in the Sahel.

A common adjective in the preceding paragraphs is "idealised": many results underpinning our understanding of MCS dynamics ultimately stem from high resolution large–eddy simulations under idealised scenarios. Yet MCSs are well simulated by kilometre–grid scale convection–permitting (CP) models, despite such models' parameterisation of many smaller scale processes (Prein et al. (2017); Crook et al. (2019)), with results for many key characteristics very similar to LES–scale models (Prein et al. (2021)). Multiple state–of–the–art global CP models can now be run on climate timescales while resolving MCSs (Hohenegger et al. (2023); Rackow et al. (2024); Donahue et al. (2024)), explicitly embedding the dynamics and forcings of MCSs into global simulations (Slingo et al. (2022); Feng et al. (2023)). Such advances in computing capabilities provide an opportunity to test questions regarding the dynamics of MCSs under far more realistic experimental configurations, including all environmental interactions, and on much larger MCS sample sizes. In this context, some CP models can now capture the observed positive feedback of shear on MCS rainfall, provided they simulate a decrease in entrainment–dilution with shear (Maybee et al. (2024)), with errors in simulated rainfall–shear response explaining spatial biases in West African MCS mean rainfall and diabatic heating.

The results of Maybee et al. (2024) highlight the importance of evaluating how MCSs interact with wind shear. The role of convective cold pools, and the surrounding debate regarding their role in MCS dynamics, was not considered. Here we focus on this question for the Sahel by comparing MCSs between two 40 day CP simulations, described

in Section 2, that differ only by the switching off of rainfall evaporation in one experiment. In Section 3 we show that convective cold pools are thus suppressed in our experiment, but despite this long–lived, mature MCSs which propagate deep into the night still form. We consider the changes to interactions with wind shear in Section 4, finding limited change in the leading–order scalings of key MCS fields (rainfall, brightness temperature) when cold pools are suppressed. We discuss how our results intersect the existing literature in Section 5, especially regarding MCS maintenance, before concluding in Section 6.

2 | DATA AND METHODS

Here we detail the two simulations ("Control" and "RainEvapOff"), MCS tracking methods (simpleTrack, Stein et al. (2014)), and key diagnostic measures used in our study. Both Control and RainEvapOff are 2.2km grid regional CP simulations conducted using the non–hydrostatic, semi–Lagrangian Met Office Unified Model (MetUM; Brown et al. (2012)).

2.1 | Experimental setup

The common modelling setup we utilise is the Limited Area Model configuration first described by Jones et al. (2023) (also LAM2.2 in Maybee et al. (2024)). The two experiments span a large North African domain (-13°–28°N, -20°–54°E) for 40 days from 01/08/2016 to 09/09/2016. Both feature a 2.2km horizontal grid spacing and 90 vertical levels up to 40km. Lateral boundary conditions are derived from a N1280 (∼10km spacing at the equator) global simulation initialised from a MetUM operational analysis, with additional forcing from daily updating SSTs. Deep convection is explicitly represented through adoption of the convection–permitting RAL3.2 science configuration (Bush et al. (2023, 2024)), which includes an explicitly represented land surface (Best et al. (2011)), a bimodal large–scale cloud parameterisation scheme (Van Weverberg et al. (2021)), and CASIM, a double moment microphysics scheme (Field et al. (2023)). For simplicity the impact of aerosols is ignored and the in–cloud droplet number concentration is fixed at ∼150 cm^{-3}, but the rain droplet number can evolve freely.

The only difference between Control and RainEvapOff stems from the CASIM microphysics scheme. In RainEvapOff, evaporation of rainfall was switched off at all levels[1]. Other species' evaporation parameters (e.g. ice, graupel) remain active, and no modifications were made in the cloud scheme. No modifications are made to CASIM in Control. An alternative compiler optimisation setting was also used for RainEvapOff, but this will not make any difference to the model diagnostics. In both simulations 2D fields were outputted on hourly timesteps, and (instantaneous) 3D fields onto pressure levels at 3 hourly intervals.

2.2 | MCS tracking

To identify MCSs and study their full lifecycle, from initiation to dissipation, we use the simpleTrack algorithm of Stein et al. (2014), which has been used extensively to track MCSs from both observational and model data (Crook et al. (2019); Tomassini et al. (2023); Feng et al. (2024)). The algorithm uses a single 2D field and tracks clusters which meet prescribed cut–off and area thresholds. We refer to individual clusters which form part of an MCS track as snapshots. To join temporally disparate clusters into storm tracks, a velocity field is calculated from cross–correlation of two contiguous timesteps. By using this field, snapshots in the earlier timestep are advected forwards to the later time.

[1] CASIM parameters `L_prevp` and `L_arevp` enabling the evaporation of rainfall were switched to `False`.

Snapshots where the fractional overlap in the later timestep between the advected and "true" cluster is greater than 0.6 are then considered part of the same storm track. A new initiation is considered to have occurred if no overlap is found with an advected cluster, while multiple advected clusters overlapping a single cluster in the later timestep is considered a merge of those storm tracks (Stein et al. (2014)).

Here we track MCSs from top–of–atmosphere brightness temperature (BT), calculated from total outgoing longwave radiation using the empirical conversion of Yang and Slingo (2001). We track storms over West Africa (here -6°–24°N, -18°–32°E) only, where the monsoon and thus MCS activity is at its peak during the simulation period. The tracking algorithm is applied to 0.1° regridded fields (equivalent to observational products), with a minimum cluster area of 9 pixels ($\lesssim$1000 km^2) and BT threshold of 241K (-32°C), as adopted in a recent intercomparison of MCS tracking algorithms (Feng et al. (2024)). Upon completion, candidate MCSs are selected as tracks where during the storm lifecycle, a maximum area >5000km^2 and minimum BT <223K (-50°C) are achieved. For these tracks, snapshot rainfall volumes and extremes are calculated from precipitation on the same 0.1° grid. MCSs are then further required to reach a maximum rainfall rate above 1mm hr^{-1} during the storm's lifetime. Finally, we restrict our attention to MCSs in the Sahel by excluding track initiations outside 9° – 19°N and -10° – 24°E.

We are particularly interested in the convective dynamics of mature MCSs, which we identify after tracking as contiguous subregions of BT below -50°C with area larger than 5000km^2 within a tracked snapshot. MCS mergers can cause individual tracked snapshots to be formed from multiple mature storm regions, where individual cores' convective dynamics are well isolated and distinct. Field composites for mature MCSs are thus centred on the location of the minimum BT (BT$_{\text{min}}$) of all distinct, unconnected mature subregions of a track snapshot. We restrict our sample of mature MCSs to those east of -12°E to avoid sampling oceanic storms.

2.3 | Process evaluation

To distinguish cold pool characteristics between Control and RainEvapOff we use buoyancy b (Tompkins (2001)), which we calculate from the virtual potential temperature θ_v:

$$b = \frac{g(\theta_v - \bar{\theta}_v)}{\bar{\theta}_v}, \tag{1}$$

where g is Earth's gravitational field and $\bar{\theta}_v$ is the mean value across a 100×100km bounding box (Prein et al. (2021)). Note that buoyancy should be calculated from density potential temperature θ_ρ, which further includes mixing ratios for cloud condensate and rain water in addition to water vapour: these microphysical diagnostics were unfortunately not available for the long simulations used here. We therefore use θ_v as the closest possible approximation. Cold pool outflow boundaries can then be approximately located by identifying regions with strong gradients in θ_v (Drager and van den Heever (2017)).

To evaluate the role of cold pools in MCS environmental interactions, we consider only mature MCS regions during the hours of peak convection (16–21 UTC) that themselves have a maximum rainfall rate >1mm hr^{-1}. We define the environmental conditions for such storms as the preceding 12 UTC mean field across a 0.7° box centred on the location of the mature MCS BT$_{\text{min}}$ (Klein et al. (2021)). As in Maybee et al. (2024) we represent MCSs' thermodynamic and dynamical environments by total column integrated water vapour (TCW) and the difference between 850hPa and 650hPa zonal winds ($u850 - u650$), respectively, where the latter measure is henceforth referred to as shear. The choice of shear measure corresponds physically to the difference between the AEJ and south–westerly monsoon flow, and roughly spans heights between 1 and 3.5km above the surface.

We follow Baidu et al. (2022) and Maybee et al. (2024) and evaluate changes in entrainment–dilution with shear

by calculating two proxies for bulk entrainment,

$$w_{eff} = \frac{w500_{max}}{\sqrt{CAPE_{env}}} \qquad \text{and} \qquad BT_{diff} = T_{anv} - LNB_{env}\,. \tag{2}$$

Here $w500_{max}$ is the maximum 500hPa vertical velocity within the mature MCS footprint; $CAPE_{env}$ is the convective available potential energy of the storm's mean environmental sounding; T_{anv} is the mean mature MCS anvil temperature, i.e. mean BT (<-50°C); and LNB_{env} is the level of neutral buoyancy of the mean environmental sounding. Together, these variables provide a consistent picture of how bulk entrainment-dilution varies: entrainment reduces the potential of a near–surface parcel to reach its theoretical maximum buoyancy. Since this reduces w and increases T_{anv} (i.e. lowers anvil heights), reduced entrainment–dilution will correspond to high w_{eff}, the efficiency of conversion of CAPE, and low BT_{diff}, the difference between anvil and LNB heights (Baidu et al. (2022); Maybee et al. (2024)). Mulholland et al. (2021) showed that growth in convective core areas with shear yields the noted decrease in entrainment. We measure convective cores using the area of the strongest contiguous subregion where w500 is greater than the 99^{th} percentile of its in–storm values (i.e. under the mature MCS footprint). Our threshold criteria for mature MCSs ensures this measure is the same as in Maybee et al. (2024).

3 | MCS LIFECYCLES

Here we examine the structure of cold pools of 18 UTC MCSs in Control and RainEvapOff, before turning to the effect of suppressing rainfall evaporation on the diurnal cycle and nocturnal propagation of MCSs. To contextualise our MCS–level results however, we begin by looking at the effect of removing rainfall evaporation on the mean atmospheric state.

3.1 | Background mean state

As expected, turning off rainfall evaporation removes the associated sub–cloud cooling. Large parts of the domain are warmer near the surface in RainEvapOff (Fig. 1a), with much of the domain south of 20°N having 0.5–2K higher mean 1.5m air temperatures. The mean depth of the temperature difference reaches at least 650hPa at all latitudes in the domain (Fig. 1b). The deepest and largest low–level temperature differences are concentrated in the Sahel (dashed box), especially in the west. RainEvapOff shows increased westerly flow across the Sahel at 850hPa (Fig. 1a), corresponding to a strengthening of the climatological winds at this level.

What of differences in atmospheric moisture? Vertical profiles of mean moist static energy (MSE) in Fig. 1c show a similar increase in RainEvapOff at low–levels in all regions except the Sahara, with the strongest differences vs Control again in the Sahel. Above 600hPa however, all regions show reduced MSE in RainEvapOff. Integrating through the column, the spatial distribution of TCW (Fig. 1d) shows higher values in RainEvapOff across most of the Sahel and south to the Gulf of Guinea coastline. However, there is a strong drying in the western Sahara (and weaker drying over orography). As implied by the MSE profiles, the increased TCW in RainEvapOff is primarily due to increased boundary layer moisture, with a slight dry bias at midlevels (Fig. S1a). This translates into raised CAPE values in RainEvapOff — for example, the distribution of environmental CAPE values preceding mature MCSs (Fig. S2) shows a significant positive shift.

RainEvapOff has higher low–level temperatures and more rainfall reaching the surface, leading to additional latent heat fluxes (contours) into a warmer lower atmosphere that can hold more vapour. A consequence of this is

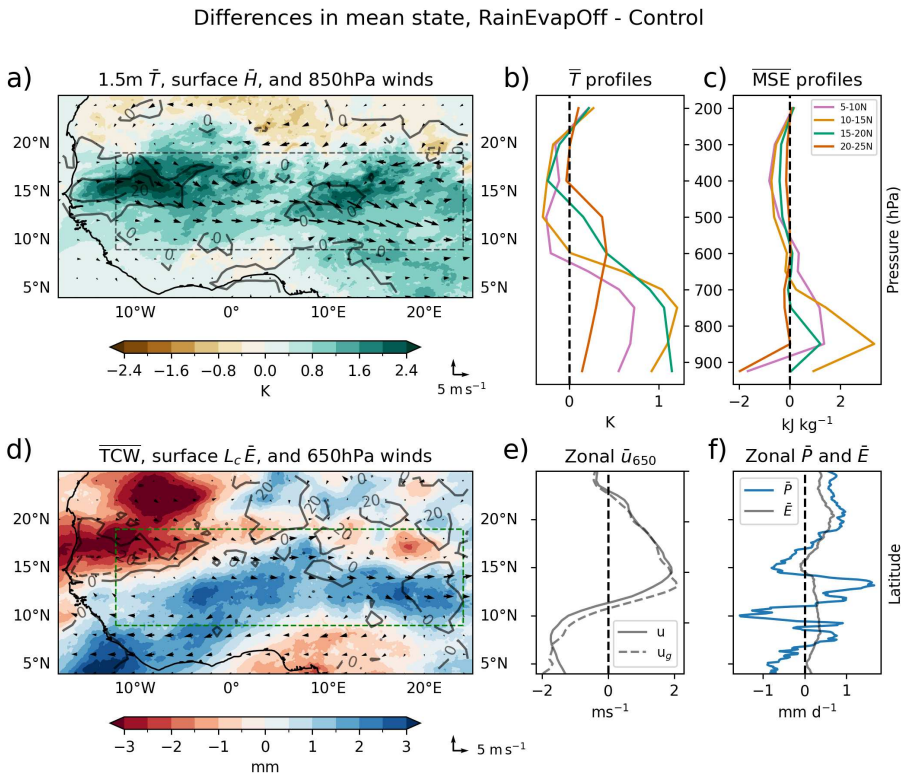

FIGURE 1 Differences between mean fields in RainEvapOff and Control. (*a*) Difference in 1.5m mean air temperature $\bar{T}$ and 850hPa wind fields (every 2° by 2°). Vertical profiles of differences in (*b*) $\bar{T}$ and (*c*) mean moist static energy $\overline{\text{MSE}}$ shown for four distinct latitude bands. (*d*) Difference in mean TCW (shading), mean surface latent heat flux $L_c\bar{E}$ (20 Wm^2 grey contours) and 650 wind fields (every 2° by 2°), accompanied in (*e*) by difference in zonal mean total and geostrophic zonal flow, u and u_g. (*f*) Difference in zonal mean daily precipitation and evaporation totals. Dashed boxes in (*a*) and (*d*) denote Sahel study region.

raised low–level humidity across the Sahel and parts of the Sahara. In contrast, mean sensible heat flux (contours, Fig. 1a) is generally higher in Control, while moisture convergence associated with the monsoon flow is similar in both simulations (S1b), pointing to the importance of surface evaporation. Mean diurnal cycles for the Sahel show consistent partitioning of the surface fluxes in the two simulations (Fig. S3), with increased Bowen ratio in RainEvapOff, but no changes to the timings of changes in low–level moisture or boundary layer depth. In addition to the role of surface evaporation and monsoon flow in enhancing low–level humidity in RainEvapOff, there may also be significant effects from the likely suppression of convective downdrafts and cold pools, which play a key thermodynamic role through injecting ambient air into the boundary layer (Tompkins (2001); Provod et al. (2016)). The differences in TCW and 850hPa winds are consistent with the drying and deepening of the Saharan Heat Low (SHL; Fig. S1c), increasing localised low–level cyclonic flow. This is consistent with a further synoptic–scale signature of cold pool suppression, since cold pools play key roles in ventilating the SHL with cool, moist air from the south (Marsham et al. (2013); Garcia-Carreras et al. (2013); Trzeciak et al. (2017)).

Comparing winds at the AEJ level of 650hPa we find that, similarly to 850hPa, winds are generally more westerly

in RainEvapOff (Fig. 1d). Here, however, this represents a slowing of the mean easterly flow. The zonal mean of the difference in 650hPa zonal wind (Fig. 1e) shows an inflection at ~12°N, with reduced easterly flow in RainEvapOff vs Control across most of the Sahel. This change is consistent with the alteration to thermal wind balance resulting from the distribution of temperature increases in RainEvapOff, as shown by close alignment with the zonal mean differences in the geostrophic component u_g. Over West Africa geopotential height is approximately a function solely of temperature; consequently, thermal wind can be described, to close approximation, by the vertically varying geostrophic flow. The changes in the zonal wind differences in Fig. 1e align with a strengthened meridional temperature gradient over 4°–12°N in Fig. 1a, and weakened gradient from 12°–20°N, the latter of which weakens the easterly flow.

Finally, Fig. 1f shows the difference in zonal mean daily precipitation totals $\bar{P}$. The design of our sensitivity experiment suppresses the loss of rainfall mass to water vapour — yet interestingly, rainfall in RainEvapOff is not higher everywhere in the monsoon region, with higher rainfall rates in Control at the coast, 10°N and 16°N. Only at 16°N can this be explained by relatively higher zonal mean evaporation $\bar{E}$ in Control. In RainEvapOff the coastal rainfall is shifted northwards, but the biggest increases are in the core Sahel band and Sahara. The latter increase is likely since the majority of rainfall would typically evaporate in the lower atmosphere under the very high temperatures and low relative humidities. The increase in the Sahel, where MCSs dominate the climatology, points to the expected increased efficiency of storm rainfall when evaporation is suppressed.

In summary, switching off rainfall evaporation causes significant changes to the West African monsoon. Across the Sahel, the boundary layer is warmer, moister and more convectively unstable in RainEvapOff, with increased latent heat fluxes compensating for decreased atmospheric evaporation. The weakened Sahara–Sahel meridional temperature gradient enhances the westerly component of the low–level monsoon flow, but weakens the mid–level easterly flow across the region. Total precipitation is increased over the Sahel, but decreases over other regions of West Africa.

3.2 | Cold pool structure

As a qualitative illustration of the fundamental differences in MCS structure between RainEvapOff and Control, Fig. 2 shows the footprint of a westward–propagating MCS at 18UTC on 01/08/2016. We use the time of peak convection on the first day for this comparison to ensure that divergence between the two experiments is still small. In the Control MCS (Fig. 2a), strong regions of negatively buoyant air at 925hPa are colocated with two intense convective updrafts demarcated by high rainfall rates. The colocation of these regions behind the linear $|\nabla\theta_v|$ contour (yellow), orthogonal to the direction of propagation, denotes the existence of a large, organised convective cold pool density current propagating ahead of the MCS convection but located within the footprint of the anvil shield (BT $= -32$°C contour, dashed). Ahead of the cold pool's leading edge, the air is very buoyant, suggesting low–level storm inflow being mechanically lifted by the cold pool.

In Fig. 2b we see that despite the MCS generating higher rainfall rates without evaporation, there is no formation of a significant cold pool. There are some small, disconnected negatively buoyant regions around the convective core, with several dispersed $|\nabla\theta_v|$ contour features nearby: these features will be generated by the evaporation of graupel and ice species. This evaporation is enough to generate some small surface cold pools, but not the large, organised density current seen in Control. There is also no clear low–level inflow region of positively buoyant air.

Figure 2c plots the difference in 925hPa $|\nabla\theta_v|$ between RainEvapOff and Control across the entire region, giving a wider view of the cold pool characteristics at this time. The region is dominated by numerous arc–shaped (open to the east) tight peaks of Control (purple) $|\nabla\theta_v|$, showing the strong changes in buoyancy associated with very large convective cold pools. In contrast, no such features are seen for RainEvapOff (orange), which are instead limited to

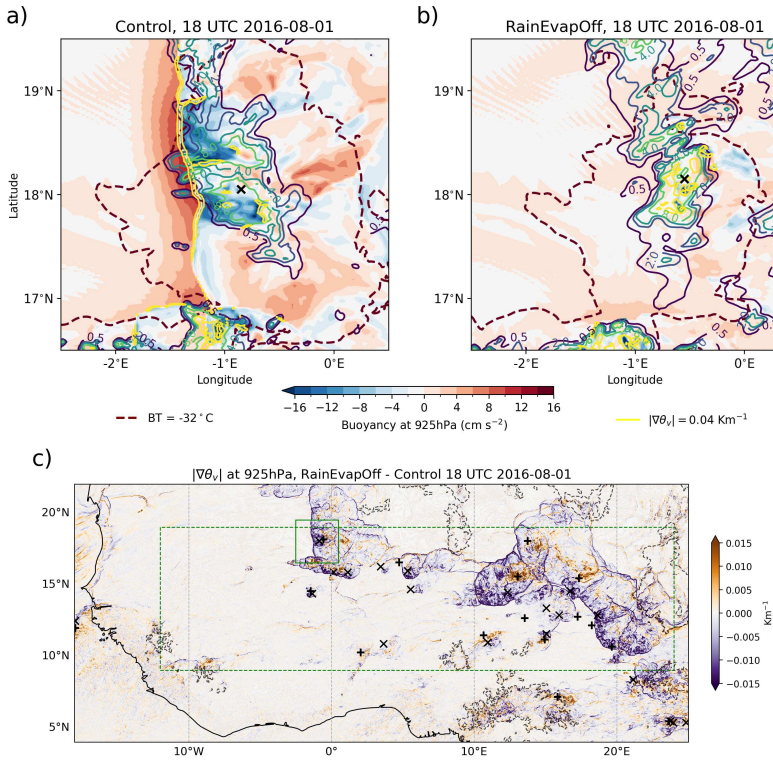

FIGURE 2 Representative MCS structures at the same location in (*a*) Control and (*b*) RainEvapOff at 18 UTC on 01/08/2016. Colour shading shows buoyancy at 925hPa (cm s^{-2}), labelled blue–green contours show mean hourly rainfall rates (mm hr^{-1}). Dashed bold contour shows MCS anvil footprint (BT<-32°C), and yellow contours show boundaries where $|\nabla\theta_v| = 0.04$ K m^{-1} at 925hPa. (*c*) Difference in $|\nabla\theta_v|$ field at 925hPa across West Africa between RainEvapOff and Control at 18 UTC on 01/08/2016. Location of tracked mature MCS BT_{min} locations at this time in RainEvapOff (Control) shown by + (×) markers. Solid green box indicates region in panels (*a*, *b*), dashed green box denotes Sahel study region. Dashed grey contours shown for surface elevations of 750m and 1500m.

tightly–bound dense clusters of contours as seen in Fig. 2b. However, this does not indicate an absence of MCSs: markers showing the locations of mature MCS locations from both simulations show a roughly comparable number of features between Control and RainEvapOff. At this early timestep there are MCSs in RainEvapOff, and they do not have canonical cold pools. Note that the dominant MCS propagation direction is westwards (i.e. easterly) across the Sahel, with less than 10% of storms in either simulations propagating east (Fig. S4a).

These illustrative results are taken for one timestep, soon after simulation initialisation. Figure 3 shows the differences in mean composite cold pool structure at 18 UTC between Control and RainEvapOff for the full 40 days. Both simulations show comparable numbers of mature MCSs, with composites taken around 462 BT_{min} locations in RainEvapOff and 415 in Control.

As anticipated, on average cold pools are stronger and larger in Control. Fig. 3a displays a ~100km westward arc focused on the composite centre where the negative buoyancy in Control is >0.8 cm s^{-2} stronger. Buoyancy is more negative for MCSs in Control everywhere 100km behind (i.e. trailing) this arc, and is more positive than RainEvapOff west of x=-50. The strongest difference in wind anomalies is colocated with the arc, with stronger easterly winds in

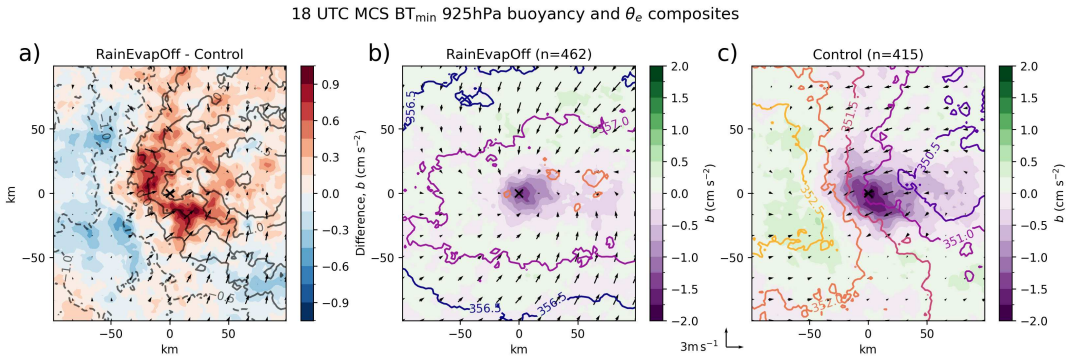

FIGURE 3 Difference (a) between (b) RainEvapOff and (c) Control 18 UTC mature MCS composite mean 925hPa buoyancy (cm s^{-1}, shading), equivalent potential temperature θ_e (0.5K contours) and spatial anomalies of storm–relative winds (m s^{-1}, common barb scale). Storm speeds taken from instant velocity values outputted by simpleTrack algorithm, with wind field coarsened for display purposes. Values n indicate composite sample sizes; composite centre "core" location marked by black cross.

Control indicative of gust fronts at cold pools' leading edges. In RainEvapOff, evaporation of graupel and ice is clearly able to generate localised negatively buoyant regions, with dense air at the composite centre and behind the mean core location (Fig. 3b). However, this "mean cold pool" is much weaker and more limited in extent than its counterpart for MCSs in Control (c.f. Fig. 3c).

The qualitative differences in cold pool structures seen in Fig. 2 are borne out in the composites. In Control there is a negative zonal gradient of equivalent potential temperature across the MCS, and easterly wind anomalies east of x=-50 only. Since low–level inflow to storms' convective cores is typically moist and convectively unstable (high CAPE), inflow is anticipated from high–θ_e regions. The fields in Fig. 3c are thus consistent with a squall line with (westerly) low–level inflow from positively buoyant air ascending over a (easterly) cold pool gust front ahead of the deep convection, and moreover agree with observations of monsoon–season MCSs (Provod et al. (2016)). Meanwhile in RainEvapOff, the θ_e gradient is positive, with peak values behind the composite centre, where a "sink" in the predominantly meridional wind anomalies lies. This points to the evolution of a very different MCS structure in the absence of rainfall evaporation, a point we investigate further in Section 4.

Figure 4a further shows the differences in composite MCS rainfall and absolute 925hPa storm–relative winds between the experiments. Close to the BT$_{min}$ core location rainfall is significantly higher in RainEvapOff than Control, as expected from our experimental design. Rates are also higher in RainEvapOff in the region of weaker stratiform rainfall east of (i.e. following) the composite centre. However, directly north and south of the centre rainfall is more than 1mm hr^{-1} higher in Control. A similar pattern is repeated in composites for brightness temperatures, with lower values in Control on this axis (Fig. S5). These results are caused by the systematic difference in MCS structure between the two experiments: large cold pools in Control form westward propagating linear squall–lines (exemplified by Fig. 2) with further convective cells on the meridional axis neighbouring the composite–centred core, in contrast to the dominant isolated features about which composites are taken in RainEvapOff. This is further evidenced in Fig. 4a by the colocation of the strongest zonal wind differences, corresponding to strengthened easterly flow in Control from the cold pool density currents, with regions where rainfall is higher in Control.

The mean effect of MCS propagation on 925hPa temperature and moisture is shown by Figs. 4b and 4c. While air is warmer everywhere in RainEvapOff (Fig. 1), this is notably enhanced over an area larger than 100km^2 close to

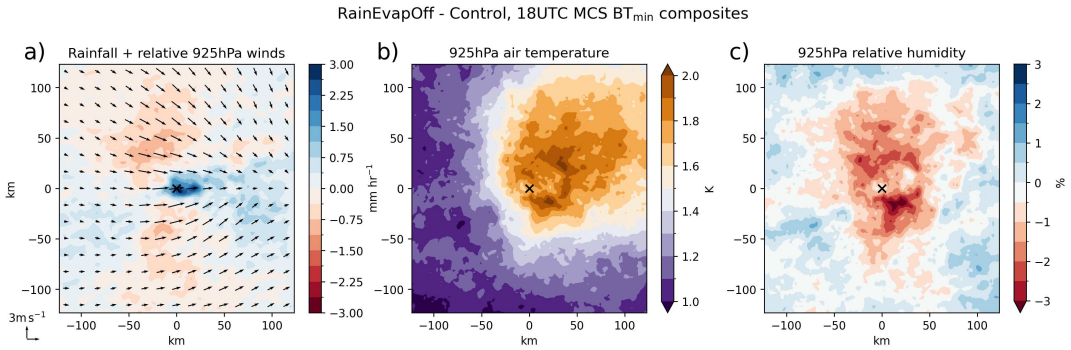

FIGURE 4 Differences in 18 UTC mature MCS composite mean (*a*) rainfall (mm h^{-1}) and 925hPa storm–relative winds, (*b*) 925hPa air temperature (K) and (*c*) relative humidity (%) between RainEvapOff and Control. Storm relative winds obtained as in Fig. 3.

and behind the core mean location, indicating the pronounced effect of the cold pools in Control on air temperatures under and behind MCSs. The central 100km^2 region is meanwhile more humid in Control (Fig. 4c), despite the higher ambient humidity in RainEvapOff shown around the composite edges. On average, MCS convection in RainEvapOff is associated with far weaker decreases in temperature, and increases in humidity, of low–level ambient air than Control. Both signals are indicators of the passage of observed Sahelian cold pools (Hoeller et al. (2024)), further showing a strong suppression of cold pools in RainEvapOff.

3.3 | Diurnal cycle

The results of the previous section confirm the expectation that removing rainfall evaporation strongly suppresses convective cold pools, at least at the diurnal peak of convection. Maybe more intriguing is the persistent ability of mature MCSs to form without these cold pools. This could be explained by short–lived convection, generated by the significant ambient convective instability in the afternoon Sahel boundary layer, which struggles to maintain the organised structures overnight. Figure 5 shows that this is emphatically not the case: the lifetimes of both experiments' MCS populations (Fig. 5a) peak at 2 hours. A weak positive effect of cold pools on longevity is suggested by 3% more storms living for 3 hours or less in RainEvapOff, versus 4% more storms living between 5 and 9 hours in Control. However, in both simulations ~15% of MCSs are long–lived storms that persist for 10 hours or more.

Figure 5b shows that MCS propagation speeds are on average lower in RainEvapOff, with a population peak 1.7 ms^{-1} lower (23%) than Control and mean speed 0.9 ms^{-1} (10%) lower — a two–sided Student's t–test verifies that the change in the means is significant (p<0.01). Here the MCS propagation speed is calculated as the geodesic distance between the initial and final track snapshot locations, divided by the number of hours between them (Crook et al. (2019)). The suppression of cold pools in RainEvapOff may yield a direct, dynamical reduction in MCS speed; however, MCS propagation speed in the Sahel is primarily determined by the steering flow of the African Easterly Jet (Bickle et al. (2021)). Approximating the AEJ strength in the experiments as the daily maximum zonal–mean easterly wind determined from a 2° rolling meridional mean from 10°–20°N, we find a significant decrease in the distribution of daily AEJ strength in RainEvapOff of 1.9 ms^{-1} (p<0.01 under t–test). This is comparable to the decrease in MCS propagation speeds. The weakening of the background 650hPa easterly winds, and thus AEJ, in RainEvapOff is due to changes in thermal wind balance resulting from increased low–level temperatures that weaken the meridional

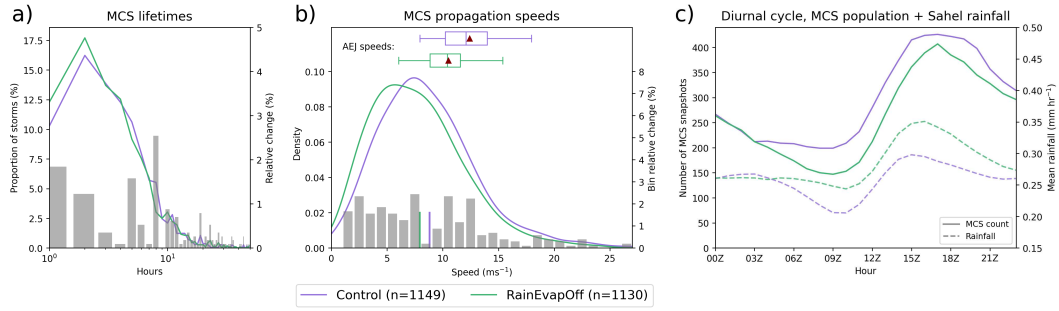

FIGURE 5 Lifecycle statistics for Sahel MCS tracks in Control (purple) and RainEvapOff (green). (*a*) MCS lifetimes binned on 1 hour intervals. Grey bars show percentage change of bin counts in RainEvapOff relative to Control. (*b*) Continuous probability density functions (PDFs, lines) and relative 1ms^{-1} bin differences (grey bars) for MCS propagation speeds; continuous PDF derived using a Gaussian kernel density estimate with a maximum value of 30ms^{-1}. Vertical lines on *x*–axis denote distribution means. Horizontal box plots show distribution of daily mean zonal AEJ speeds, with distribution means indicated by triangles. (*c*) Hourly total counts of tracked MCS snapshots (solid lines) and mean Sahel rainfall (dashed). Values *n* in legend specify number of independent MCS tracks.

temperature gradient (Fig. 1). The primary influence of cold pools on the MCS speeds is thus likely indirect, through their contribution to the mean thermodynamic state. Note that the MCS speeds are derived from the OLR field alone, and may differ to that of the cold pool density currents.

The continued nocturnal maintenance of MCSs in RainEvapOff is confirmed by the diurnal cycle of the MCS snapshots that piece together the storm tracks (Fig. 5c, solid lines). The timing and gradients of the cycles are generally similar, reflecting similar initiation and dissipation rates (Fig. S2); the two count distributions are equivalent under a two–sample KS test (p=0.26). While the shape of the diurnal cycle of the MCS populations mirrors that of all rainfall over the Sahel (Fig. 5c, dashed lines), total regional rainfall is higher in RainEvapOff except around 00 UTC. However, fewer storms persist into the early hours of the morning in RainEvapOff. There is a divergence in storm counts after 03 UTC, with RainEvapOff showing 26% fewer MCSs at the diurnal minimum of 09 UTC. This is despite an increase in regional rainfall versus Control — individual MCSs fractionally contribute higher rainfall amounts in RainEvapOff at this time. Note morning initiation rates are also higher in Control (Fig. S2b), where cold pool outflows provide local convergence lines which aid convective development, and the peak in regional rainfall is earlier in the day, consistent with the role of cold pools in allowing upscale organisation. These differences not withstanding, nowhere does the MCS count in either simulation get close to zero, with the RainEvapOff minimum still corresponding to persistence of more than 4 MCSs a day on average.

The different behaviour of early morning storms in RainEvapOff is reinforced by mean diurnal cycles plotted in Fig. 6. In Control, a nocturnal (03 UTC) peak in MCS area, total and maximum rainfall, and accompanying secondary minimum in BT, points to intense MCSs at that time, consistent with observations (Vizy and Cook (2018)). This peak is missing for RainEvapOff, which shows a single, lower diurnal minimum in MCS BT driven by primary storm initiation and fuelled by higher environmental CAPE (Fig. S2); relatively constant maximum rainfall rates; and highest total rainfall amounts during the period of least convective activity. The peak in mean storm area is 16% lower and 2 hours earlier than in Control. Together, these differences show that inhibiting rainfall evaporation suppresses mechanisms through which nocturnal MCSs can continue to intensify after the peak in convective activity. In RainEvapOff only the strongest, largest storms continue to propagate beyond early morning, leading to the markedly later peak in total storm rainfall.

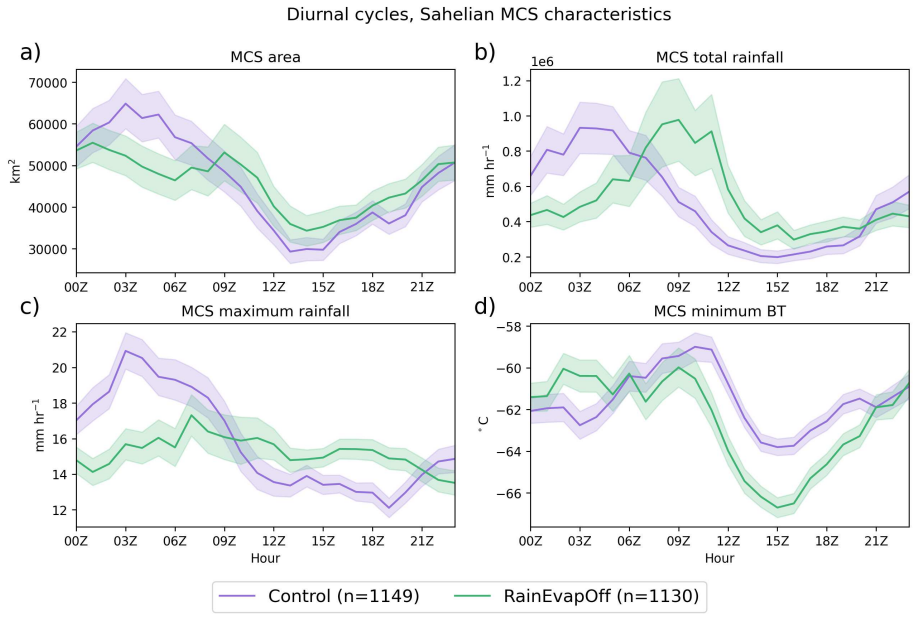

FIGURE 6 Mean diurnal cycles of tracked Sahelian MCS (*a*) snapshot anvil areas (km^2), (*b*) total rainfall (sum of rainfall rates within MCS area; mm hr^{-1}), (*c*) maximum rainfall (mm hr^{-1}), and (*d*) minimum BT (°C) in Control (purple) and RainEvapOff (green). Shading denotes standard error on the mean. Hourly means taken excluding values above the hourly 95th percentile for areas and rainfall to exclude interference from outlier values. All values calculated from 0.1° regridded fields.

To understand the role of cold pools in the simulations' differing nocturnal MCS convection, Fig. 7 shows the overnight evolution of the differences in cold pool buoyancies between RainEvapOff and Control. The 18 UTC mean composites (panel a) again display enhanced differences in buoyancy west of the composite centre location; stronger differences in θ_e to the east; and enhanced RainEvapOff rainfall at the centre only. The distribution of MCS minimum buoyancy values (panel d) is skewed towards more negative values in Control, indicating stronger buoyancies in Control stemming from large density currents beneath Control MCSs (e.g. Fig. 3). This same qualitative pattern is maintained throughout the night in both spatial means and PDFs: the nocturnal maintenance and propagation of MCSs in RainEvapOff is not explained by a small number of storms developing strong cold pool features.

There are however some important nocturnal changes. At midnight the difference in mean buoyancy is even stronger (Fig. 7b): a strengthening of negative cold pool buoyancy in Control is responsible, with a peak in minimum buoyancy developing at -12 cm s^{-2} (panel e) in Control only. A similar result holds for the distribution of mean buoyancy (Fig. S6). This intensification explains the appearance of a dipole in rainfall differences, with a region of enhanced rainfall in the Control MCSs west of the centre (contours, Fig. 7b). In all, the 00 UTC MCSs in Control show strengthened cold pools simultaneous to early–morning peaks in MCS rainfall and BT (Fig. 6) that are absent in RainEvapOff. This indicates that the growth of large, organised convective cold pools is the mechanism driving the nocturnal peaks seen in Control. At 06 UTC (Figs. 7c and f) the cold pool density currents in Control weaken relative to 00 UTC, but remain much stronger than counterparts in RainEvapOff.

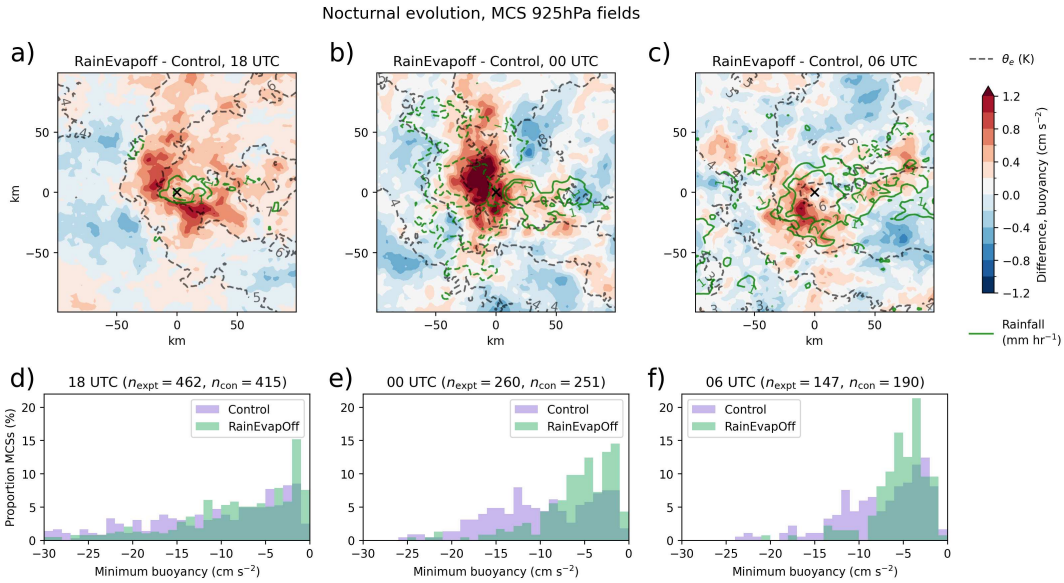

FIGURE 7 $(a-c)$ Differences in mature MCS composite mean 925hPa buoyancy (shading, cm s−2), 925hPa equivalent potential temperature (dashed grey 1K contours), and surface rainfall (green 1mm hr^{-1} contours) between RainEvapOff and Control at 18 UTC, 00 UTC, and 06 UTC. $(d-e)$ Histograms of minimum 925hPa buoyancy at the same times, sampled within 100km box centred on mature MCS core locations.

4 | INTERACTIONS WITH WIND SHEAR

Cold pools are thought to play an important role in the interaction of mature MCSs with vertical wind shear (Thorpe et al. (1982); Rotunno et al. (1988)). Here we investigate the effect of suppressing cold pools on MCS updraft structure and shear–controls on MCS rainfall.

4.1 | Updraft structure

We begin by comparing the zonal mean geometry of MCSs in Control and RainEvapOff. Figure 8 shows composite zonal mean vertical sections centred on 18 UTC mature MCSs in both experiments, i.e along the y=0 line for horizontal composites in Figs. 3 and 4. The profile of horizontal convergence for MCSs in RainEvapOff (Fig. 8a) shows a vertical region of strong convergence along the x=0 axis (dashed red). At low levels the strongest convergence is behind (east of) the centre line, extending up to 850hPa for nearly 100km; vertical velocities (grey contours) peak around 400hPa at x=0. The region of ascent is tilted slightly forwards, in the direction of propagation, with the convergence field suggesting low–level inflow primarily in the ∼75km behind the composite centre.

This picture is confirmed by the mean zonal (composite anomaly) θ_e field, in which positive anomalies on a given level indicate relatively moist, warm air. Above 600hPa, positive anomalies are focussed around the x=0 line, colocated with the strongest vertical velocities in Fig. 8a. Below 700hPa however we see stronger positive anomalies behind the centre point (as in Fig. 3b), further indicating this region is the source of low–level inflow air for the MCS's convective updrafts. Contours of buoyancy show that any localised negatively buoyant is weak and restricted to below 875hPa.

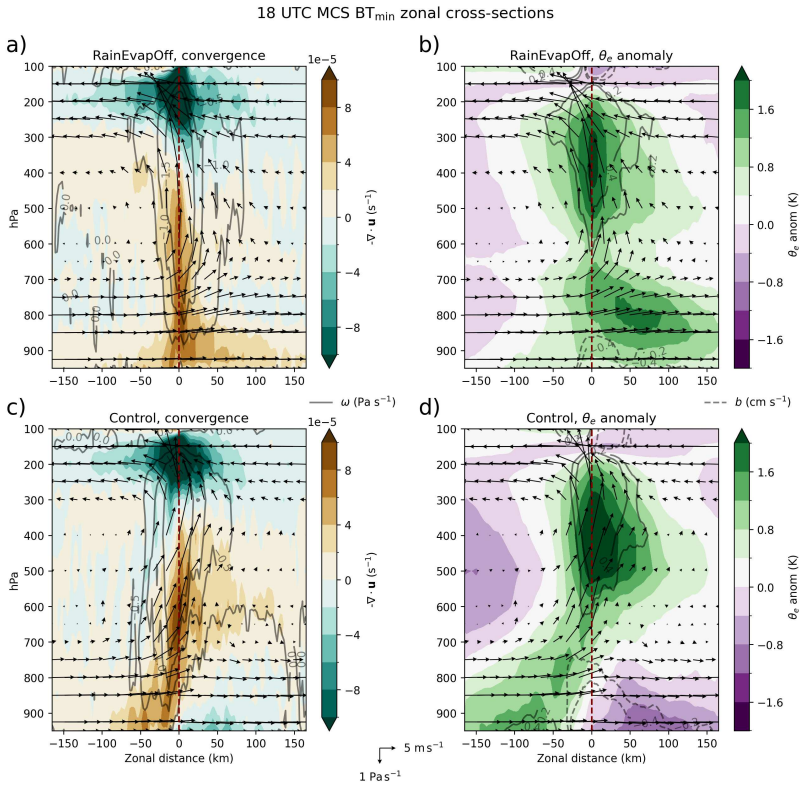

FIGURE 8 18 UTC composite mean zonal sections over central 50km transect for mature MCSs in RainEvapOff (top row) and Control (bottom row). Panels (a) and (c) show mean horizontal convergence (shading) and vertical velocity ω in pressure coordinates (0.2Pa s^{-1} contours); panels (b) and (d) show mean equivalent potential temperature anomaly (shading) and buoyancy b (0.2cm s^{-1} contours), where θ_e anomaly is taken against the mean composite profile. Wind barbs show ω and storm–relative zonal wind components on common scale in plane of cross section; storm–relative winds taken from instant velocity values outputted by simpleTrack algorithm. Zonal wind field coarsened for display purposes.

MCSs in both experiments show divergent flow at 200hPa above and ahead of the x=0 line, indicating outflow from deep–convective updrafts at the LNB. However, at mid and low levels the vertical structure for MCSs in Control is very different. The region of strong convergence (Fig. 8c) is primarily ahead of the composite centre near the surface, tilting backward for 100km before straightening vertically above 650hPa. Strong vertical ascent is found in this region and at all levels above, again peaking around 400hPa. The 150km east of the centre shows weak descending air, with ω>0 below 650hPa and divergent flow below 800hPa, indicating the presence of widespread convective downdrafts. Buoyancy contours in Fig. 8d show the associated formation of deep convective cold pools at the surface, with a clear density current feature out to x=-100km in the zonal mean.

The distribution of raised θ_e anomalies further points to backwards tilting updrafts, over the surface cold pool density current, with low–level inflow sourced ahead of the MCS convection. The relative differences between the updraft and ambient air θ_e values are stronger in Control than RainEvpOff, with generally higher buoyancies (both positive and negative), indicating stronger environmental contrasts and increased subsidence in Control, which shows

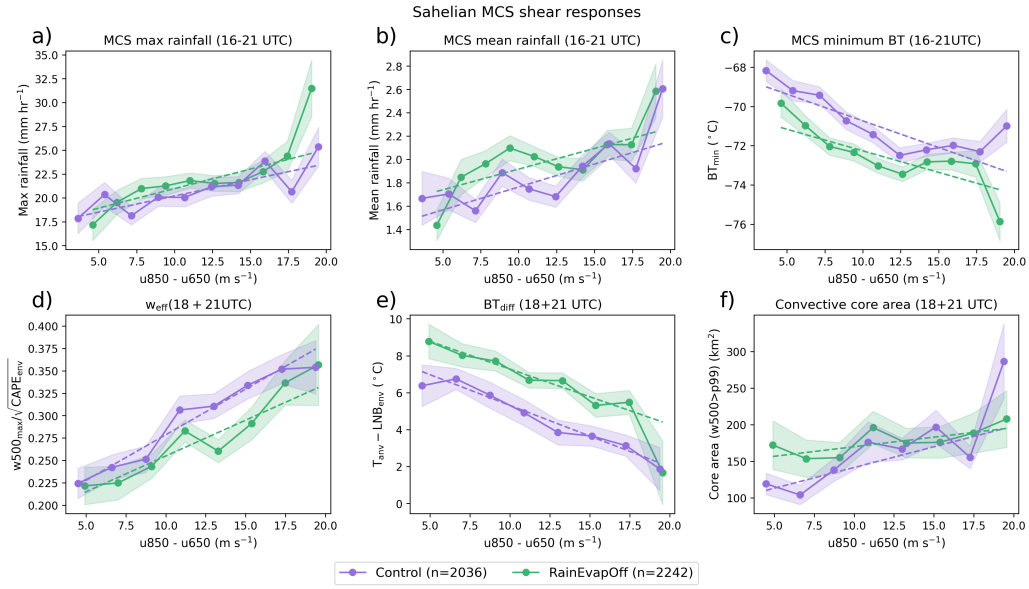

FIGURE 9 $(a-c)$ 16–21 UTC maximum rainfall, mean rainfall and minimum BT, respectively, for mature MCSs with maximum rainfall >1mm hr^{-1}, binned by 12 UTC environmental shear. Bins calculated between 5th and 95th shear percentile to remove extremes.$(d-f)$ 18+21 UTC MCS entrainment proxies w_{eff} and BT_{diff}, and 500hPa core areas, similarly binned by shear. Difference in times due to 3 hourly profile fields; values n indicate MCS sample sizes from 16–21UTC. In all plots shading denotes standard error on bin mean, and dashed lines indicate trend for error–weighted regression where gradient and correlation are significant at 95% level.

mid–level divergence ahead of the convective region (panel c). However, close to the composite core updraft velocities are stronger at nearly all levels for MCSs in RainEvapOff (Fig. S7a), with mean 500hPa ω=-4.23Pa s^{-1} in a 25km square about the composite centre, vs -3.28Pa s^{-1} in Control. The stronger updrafts in RainEvapOff are a consequence of stronger low–level convergence than in Control (Fig. S5b), and the significantly higher environmental CAPE values (Fig. S2) due to the moister, warmer mean state.

The holistic differences in mean updraft structure between RainEvapOff and Control remain consistent through MCSs' nocturnal propagation, and we find far less pronounced differences in the meridional vertical composites, which are typically symmetric about the $y = 0$ axis (not shown). This is to be expected from the primarily westwards propagation of MCSs in both experiments, aligned with the strongest shear. Despite showing a weaker AEJ (Fig. 5b), RainEvapOff shows very similar zonal shear values to Control due to the complimentary enhancement in low–level westerlies (Fig. 1). The differences in the updraft structures, and tilt in particular, are thus consistent with RKW theory (Rotunno et al. (1988)), with the convective cold pools in Control providing negative meridional vorticity at low–levels and thus partly balancing the shear. In RainEvapoff there is no such balance and the tilt is forwards, although an absence of updraft weakening is in part due to the modified environmental conditions.

4.2 | MCS environmental response

Given the pronounced differences in mean updraft structure and shear interaction, the control of shear on the strength of MCS convection, measured through characteristics such as rainfall and BT, may be anticipated to also differ significantly between the experiments. Figure 9 shows this is not the case. The scalings of mature 16–21 UTC MCS maximum rainfall (Fig. 9a), mean rainfall (Fig. 9b) and minimum BT (Fig. 9c) with 12 UTC environmental shear strength are remarkably similar in the two experiments. For maximum rainfall the scaling is ~20% stronger in RainEvapOff, and while ~10% and ~20% weaker for RainEvapOff MCS mean rainfall and minimum BT, respectively, there is no collapse in the shear response due to the absence of cold pools. Both experiments show similar dependence on TCW (Fig. S8), but do have differing MCS number distributions (Fig. S9), with stronger background shear in Control and a tighter clustering of MCSs near the mean AEJ speed in RainEvapOff.

We have previously shown that the increase of MCS rainfall with shear in Control (LAM2.2 in Maybee2024) is explained by a decrease in bulk entrainment–dilution. Here we find that this hypothesis remains true when rainfall evaporation is removed: Figs. 9d and 9e consistently show reduced bulk entrainment at high shear, with increased w_{eff} and decreased BT_{diff} values in these environments. The reduction of entrainment–dilution with shear explains the scalings of MCS rainfall and BT_{min} in both experiments, with significant correlations against the shear–binned entrainment measures. That this remains the case in RainEvapOff, where cold pools are strongly suppressed and there is no horizontal vorticity balance, indicates that entrainment–dilution effects are the leading–order mediator of shear controls on mature MCS convection.

There are important sub–leading effects apparent from the suppression of cold pools, however. The entrainment–dilution scalings are weaker in RainEvapOff, with consistently lower w_{eff} and higher BT_{diff} values indicating higher bulk entrainment, likely a consequence of the drier mid–level mean state in RainEvapOff (Fig. S1a). The positive feedback of cold pools is most apparent in the scaling of MCS convective core areas in Fig. 9f, the growth of which with shear is understood to facilitate the reduction in entrainment rates (Mulholland et al. (2021)). Both experiments show a positive feedback of shear on core area size; however, the scaling in RainEvapOff is much weaker (half that in Control). This points to an important dynamical influence of MCS cold pools on updraft widths, and thus entrainment–dilution, leading to sub–leading effects on MCS rainfall. Cold pool intensities typically increase with shear due to intensified rainfall evaporation (Abramian et al. (2022)), indicating a positive feedback of cold pools on MCS updrafts.

The intensification of MCS convection with environmental shear in both experiments agrees with previous results from observations (Klein et al. (2021); Hsiao et al. (2024)); in contrast, an older MetUM climate simulation, CP4–Af, showed extremely weak shear controls on entrainment and rainfall (Senior et al. (2021); Maybee et al. (2024)). Revisiting speculations in Maybee et al 2024, our results here do not indicate that improvements in the MetUM microphysics parameterisation scheme, in particular the introduction of the two–moment CASIM scheme in the present RAL3 configuration, are responsible for this improvement in the MetUM. The primary influence of CASIM on the MCS shear response is expected to be through its essential role in generating cold pools, the suppression of which we have found does not weaken shear controls.

5 | DISCUSSION

In comparing MCSs between Control and RainEvapOff, two results stand out: there is no statistically significant difference between the diurnal cycles of MCS numbers in Control and RainEvapOff, with continued nocturnal maintenance and propagation of storms without rainfall evaporation (Fig. 5); and suppressing cold pools makes little change to the dependence of MCS characteristics on shear (Fig. 9), despite changes to storms' structures. The primary changes

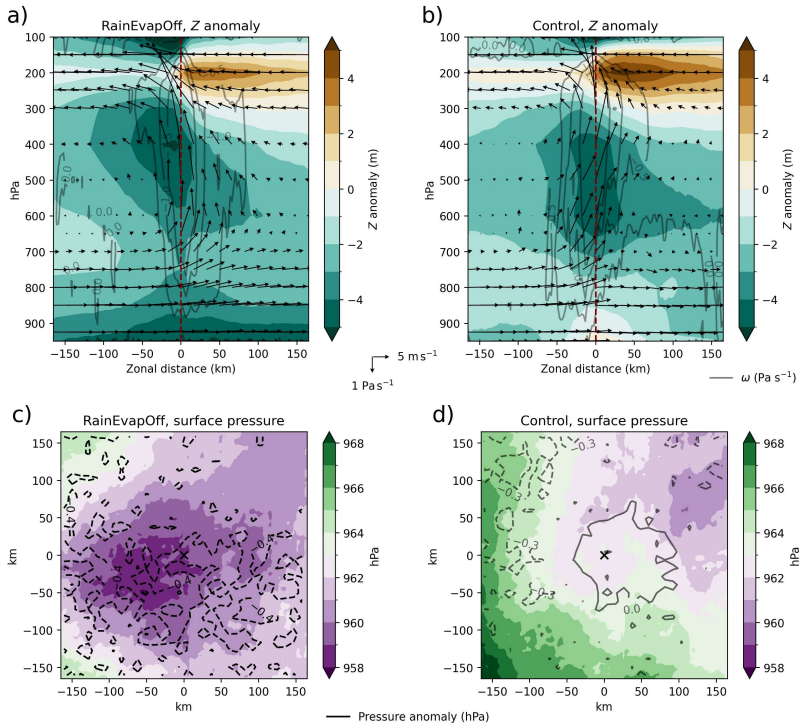

FIGURE 10 18 UTC composite means of pressure field for mature MCSs in (*a*, *c*) RainEvapOff and (*b*, *d*) Control. Top row shows mean zonal section over 50km central transect of geopotential height (Z, shading) anomaly and vertical velocity ω in pressure coordinates (0.2Pa s^{-1} contours). Data plotted on pressure levels, with wind barbs as in Fig. 8. Bottom row shows absolute (shading) and anomalous (contours) surface pressure (hPa). In all panels, anomalies are calculated against simulation mean 18 UTC climatology.

stemming from cold pool suppression are instead to the diurnal cycle of rainfall, and vertical strucutre of storms. These results are derived from large–domain CP simulations which include realistic land–surface and radiation interactions.

To understand these results, firstly consider the maintained generation of Sahelian MCSs. The mechanical lifting provided by convective cold pools is often an essential component of convective initiation (Khairoutdinov and Randall (2006); Torri et al. (2015)). In the Sahel, results from observations and CP simulations point to a key role of localised convergence (Dione et al. (2014); Birch et al. (2014a)), such as that generated along cold pool gust fronts (Maurer et al. (2017)). However local boundary layer convergence can be generated independently, for example through deep daytime rolls (Dione et al. (2014)), strong gradients in soil moisture (Taylor et al. (2011)), or by shifts in the Sahel Inter Tropical Discontinuity (ITD) dryline (Vizy and Cook (2018)). The synoptic flow provides a further crucial control, with larger–scale (300km) convergence associated with 80% of initiations in a 40 day simulation (Birch et al. (2014a)). Thermodynamical changes to the mean state in RainEvapOff independently support MCS initiation. Enhanced latent heat fluxes into a warmer atmosphere raise boundary layer moisture, yielding significantly enhanced CAPE values (Fig. S2) for developing convective cells to access. Overall, the development of equivalent MCS numbers in RainEvapOff highlights the ability of mechanisms other than cold pools to contribute to triggering convection in the Sahel, with the increase in accessible CAPE in particular catalysing strong deep convective storm development.

Once mature, cold pools are not an essential component for developing an MCS. Pandya and Durran (1996) have shown that mature squall lines' mesoscale circulation can be generated by the strong thermal forcing provided by convective rainfall alone, solely through the non–linear dynamics of gravity waves. The enhanced convective rainfall in RainEvapOff ensures such thermal forcing remains readily available, although the modified storm geometry may change the resultant circulation. Ultimately though, the steady state zonal circulation of a mature MCS is understood to depend fundamentally on a decrease in hydrostatic pressure around the updraft at midlevels, i.e. a meso–low, proceeded by a meso–high at upper levels over the trailing stratiform region (Moncrieff (1992); Yang and Houze (1996); Houze Jr (2004)). Figures 10a and b show that composite zonal sections of MCSs in both RainEvapOff and Control exhibit this structure, with negative geopotential anomalies at 500hPa in the updraft region, and positive anomalies near the tropopause behind the composite core. The generation of these pressure anomalies is independent of the storms' cold pools, whose primary effect is at the surface: in Control (panel d) the cold pool causes a region of anomalously high pressure, with a fall of pressure in the later wake of the storm. In contrast, in RainEvapOff there is no surface high and low pressure precedes the MCS. This change does not affect the initiation of deep convection, due to the existence of other triggering mechanisms, and does not disrupt convective organisation generating the intrinsic mesoscale circulation of an MCS aloft.

Sustaining the steady–state MCS circulation in Fig. 10 requires system propagation to maintain convectively unstable low–level inflow (Houze Jr (2004)). Density current outflows provide only one of multiple such mechanisms. In the midlatitudes, squall–lines can be maintained without cold pools where frontal dynamics or other mesoscale circulations provide low–level ascent (Stoelinga et al. (2003); Schumacher (2009); Trier et al. (2011)). Meanwhile in the tropics, coupling to external gravity waves can enable propagation (Crook and Moncrieff (1988); Mapes et al. (2003)), especially for fast westward–moving tropical squall lines (Tulich and Kiladis (2012)). In low CIN environments, convective interactions with internally–generated gravity waves can control the maintenance and propagation of deep convection (Mapes (1993); Liu and Moncrieff (2004); Tulich and Mapes (2008); Lane and Zhang (2011)). In particular, Grant et al. (2018) studied the relative role of cold pools and gravity wave interactions in maintaining mesoscale convection in idealised, weak–shear oceanic domains, and found that suppressing cold pools caused no change to MCS propagation and speeds, indeed enhancing storm intensity, in a striking parallel to our results for the Sahel.

In contrast though, the Sahel is a strongly sheared tropical environment. Here, MCS initiation is controlled by large–scale, low–level convergence, which is observed to continue to influence the propagation of mature MCSs (Klein and Taylor (2020)). Large–scale convergence was shown to impact idealised MCSs by Crook and Moncrieff (1988), where in experiments with no rainfall evaporation, convergence enabled the maintenance of convection despite the absence of cold pools. We find that this mechanism consistently explains our results showing the continued nocturnal propagation of Sahelian MCSs when rainfall evaporation is inhibited. Figure 11a shows that at 00 UTC, RainEvapOff indeed exhibits large–scale (300km mean) convergence at 925hPa across most of our Sahel study domain. In contrast, in Control the wind field is generally divergent. The low–level flow in RainEvapOff is thus conducive to MCS maintenance through the mechanisms of Crook and Moncrieff (1988).

This difference between the Sahelian low–level flows in the two experiments is not a static feature, instead displaying a marked diurnal evolution. Figure 11b shows the strengthened zonal mean convergence in RainEvapOff is limited to between approximately 12° and 18°N, and strongest between 17 and 05 UTC, precisely the hours of peak MCS convection (Fig. 5c). Both models' winds show similar diurnal cycles outside this core Sahel latitude band. Within the Sahel band, in RainEvapOff strong convergence preceeds peak convective initiation at 15 UTC. A weakening in convergence accompanies the growth in MCSs, but overall the mean flow remains primarily convergent, with convergence strengthening from midnight. In contrast, Control shows weakened convergence preceding 15 UTC, followed by the development of an eye of strong mean divergence at 16 UTC which lasts through the night. This flow pattern

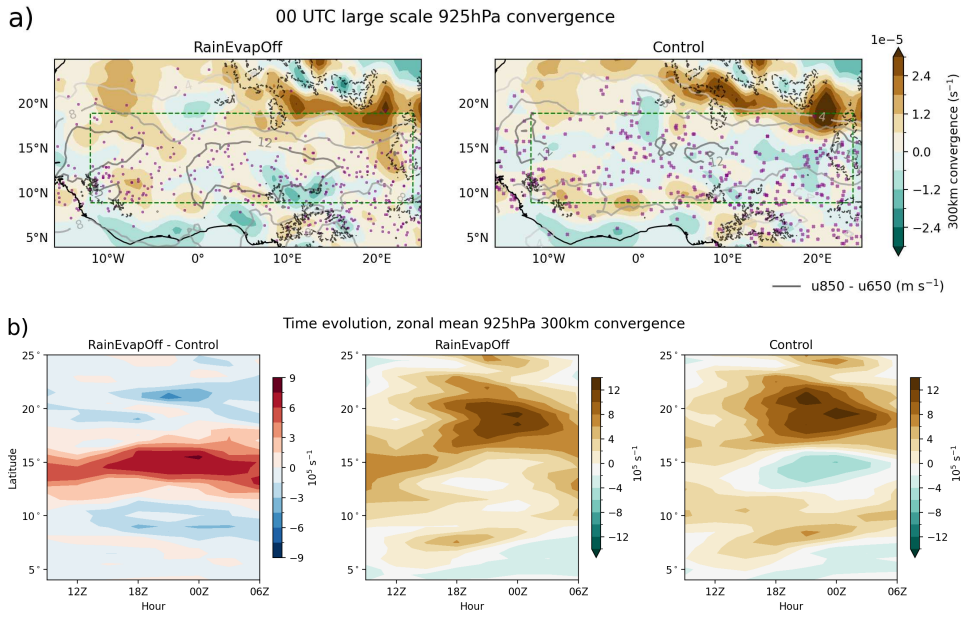

FIGURE 11 (*a*) Mean 300km 00 UTC convergence at 925hPa in RainEvapOff and Control. Means near orography (dashed contours, 750m and 1500m elevation) outside of core Sahel domain (dashed box) include winds interpolated from surface using local lapse rate where surface pressure <925hPa. Solid contours and purple markers plot mean zonal shear and mature MCS BT_{min} locations for storms with maximum rainfall > 1mm hr^{-1} at 00 UTC, respectively. (*b*) Hovmöller diagrams for diurnal cycle of difference and absolute values in mean zonal 925hPa convergence, 07 UTC to 06 UTC.

is consistent with model and observational results from Vizy and Cook (2018).

The decrease in convergence at MCS storm–track latitudes in both experiments, simultaneous to the development of mature storms, suggests an imposition of convective downdrafts on the background flow. In RainEvapOff where resultant cold pool outflows are significantly suppressed, the effect is more muted and the overall mean flow remains convergent. In Control however, where significant cold pools develop and intensify overnight (Fig. 7), there is mean divergence at low levels. We find little difference in the mean convergence at 850hPa (Fig. S10), pointing to the key role of the strong surface density currents in Control. However, related changes in the position of the ITD dryline between the models will also be a significant factor (Vizy and Cook (2018)). The inhibition of cold pool development in RainEvapOff maintains the background large–scale convergence associated with MCS initiation (Birch et al. (2014a)), and thus conditions suitable for maintenance of MCSs without cold pools (Crook and Moncrieff (1988)).

The mean flow in Control is, of course, far more realistic than that in the RainEvapOff sensitivity experiment. Cold pool density currents weaken the overall monsoon flow into the Sahara, and their misrepresentation is a key source of regional model biases (Marsham et al. (2013); Garcia-Carreras et al. (2013)). For real MCSs, whose properties and shear responses are well simulated by the Control simulation (Maybee et al. (2024)), our results show the key role of RKW vorticity balance in determining storm geometry. However, they also show that mature MCSs could equally be supported in this strong shear environment without any such balance (absent in Figs. 8 and 10); and that RKW theory does not determine the control of shear on MCS intensities, as measured by rainfall rates, updraft velocities and BT minima. The results in Fig. 9 provide further support to the hypothesis that it is the modulation of low–level inflow by

shear which is key to this control (Alfaro (2017); Bickle et al. (2022)), by showing that the (complementary) reduction of entrainment–dilution in high shear environments (Mulholland et al. (2021)) remains strong when cold pools are suppressed, maintaining a strong MCS shear response.

6 | CONCLUSIONS

Faced with significant uncertainties in future Sahel rainfall projections from models, our conceptual understanding of the underlying mechanisms serves an important role in guiding decision making. Cold pools play a pivotal role in the Sahel's climate through ventilation of the Sahara and transport of moisture (Trzeciak et al. (2017)). Disentangling their role in the observed, dynamically–driven intensification of Sahel MCS rainfall (Taylor et al. (2017)), and contribution to MCS rainfall shear–response in convection–permitting (CP) models (Maybee et al. (2024)), fills key missing gaps in our knowledge of the region's mechanisms.

We have targeted the role of cold pools in Sahel MCS dynamics through a 40 day CP MetUM simulation, RainEvapOff, in which rainfall evaporation was switched off in the CASIM microphysics scheme. Compared to an unmodified Control experiment, MCSs in RainEvapOff show significantly suppressed cold pools, with an accompanying decrease in the low–level gust front, relative humidity and temperature drop associated with the passage of an MCS. Rainfall rates are increased during the day and near the regions of most intense convective activity, but organised cold pools in Control facilitate higher nocturnal mean rainfall rates and more widespread regions of high rainfall within MCS footprints. The former result is due to an intensification in cold pool strength overnight (Fig. 7), while the latter likely stems from the generation of linear lines of convection along strong cold pool boundaries in Control (Fig 2).

Using the simpleTrack storm tracking algorithm (Stein et al. (2014)) we find sustained nocturnal propagation of MCSs where cold pools are suppressed. Similar numbers of very long–lived (>10 hours) storms are found in both experiments, while the number of MCSs in RainEvapOff only declines significantly versus Control after 03 UTC in the morning, but still with on average 4 storms a day persisting at 09 UTC within the Sahel. The primary afternoon initiation of storms is unaffected by cold pool suppression due to elevated environmental CAPE values stemming from the wetter, warmer boundary layer in RainEvapOff (Fig. S2), and the continued presence of local convergence features independent of cold pools. There is an overall decrease in the distribution of MCS propagation speeds, which we find is explained by a decrease in the speed of the African Easterly Jet (AEJ). Decreased sub–cloud cooling in RainEvapOff raises air temperatures in the Sahel, decreasing the temperature gradient with the Sahara and thus decreasing the geostrophic easterly flow. The suppression of cold pool outflows enhances the strength of the Saharan Heat Low. The changes in the mean state in RainEvapOff are fully consistent with, and provide a test of, results from the Cascade project highlighting the upscale impacts of convective cold pools on African climate (Marsham et al. (2013); Birch et al. (2014b); Garcia-Carreras et al. (2013)).

Suppressing cold pools drastically changes MCS updraft geometry (Fig. 8), as anticipated by RKW theory (Rotunno et al. (1988)), but yields no significant change in the control of environmental wind shear on MCS rainfall. Viewed together with our knowledge of storm lifecycles in the two experiments, we conclude that cold pools play a pivotal role in Sahelian MCS structure — but are not fundamental to their maintenance, and do not control their environmental interactions. Tellingly, storms in both simulations show the mid–level pressure decrease across their updrafts (Fig. 10) that is characteristic of mesoscale circulations (Moncrieff (1992); Houze Jr (2004)). Suppressing cold pools enables other dynamical mechanisms to maintain mature storms, continuing to enable the propagation of the long–lived MCSs which dominate the Sahel's climate.

In particular, our results point to the role of large–scale low–level convergence (Fig. 11) and thereby gravity wave

dynamics (Crook and Moncrieff (1988)). Divergent flow from cold pool development weakens the background convergent flow that is crucial for convective initiation (Birch et al. (2014a); Vizy and Cook (2018)) and propagation (Klein and Taylor (2020)) in the Sahel: eliminating rainfall evaporation suppresses this negative feedback and maintains a flow state conducive to MCS maintenance without RKW vorticity balance, as previously documented in other tropical and midlatitude domains (Stoelinga et al. (2003); Grant et al. (2018)). In the Sahel, Tulich and Kiladis (2012) have shown fast–propagating squall lines can be better described as convectively–coupled equatorial gravity waves — the detailed interactions between gravity waves and MCSs in our simulations is an important topic for future research. Meanwhile it would be interesting to explore similar CP experiments to RainEvapOff in other MCS hotspots globally, for example building on sensitivity experiments conducted over Taiwan (Miao and Yang (2020)).

The cold pool sensitivity experiment presented here holds two important real–world conclusions. The first is a reinforcement of the role of the AEJ in guiding MCS propagation in the Sahel: the thermodynamic mean–state consequences of suppressing rainfall evaporation weakens the jet, causing a decrease in MCS propagation speeds. The second physical conclusion is that the intensification of MCS rainfall in stronger shear environments occurs independently of cold pools. The physics of updraft entrainment, and thus convective low–level inflow (Mulholland et al. (2021); Alfaro (2017)), are the dominant mechanism. The nuanced interactions between real MCSs and vertical shear cannot be reduced solely to cold pool dynamics.

Acknowledgements

This research was conducted through the NERC funded LMCS project (NE/W001888/1). CK also acknowledges funding from the NERC independent research fellowship COCOON (NE/X017419/1). The authors thank Kilian Hermes, Mitch Moncrieff, Fran Morris, Simon Peatman, Alison Stirling and Lorenzo Tomassini for discussions which contributed to this work's progress, and Jennie Bukowski and an anonymous reviewer for thorough reviews which strengthened the manuscript. BM further thanks the Royal Meteorological Society for the award of a Rupert Ford travel grant that facilitated the development and dissemination of our results. Special thanks go to the providers of the python packages scipy, xarray, and metpy. This work used JASMIN, the UK national collaborative data analysis facility, and the Met Office MASS data archive.

Data availability statement

Access to simulation data can be provided through the JASMIN data analysis facility. The simpleTrack MCS tracking code is available at https://github.com/thmstein/simple-track, and output MCS tables and other supporting code at https://github.com/BMaybee/MCS_shear_evaluation/tree/main/Cold_pools.

References

Abramian, S., Muller, C. and Risi, C. (2022) Shear-Convection Interactions and Orientation of Tropical Squall Lines. *Geophysical Research Letters*, **49**, e2021GL095184.

— (2023) Extreme precipitation in tropical squall lines. *Journal of Advances in Modeling Earth Systems*, **15**, e2022MS003477.

Alfaro, D. A. (2017) Low–tropospheric shear in the structure of squall lines: Impacts on latent heating under layer–lifting ascent. *Journal of the Atmospheric Sciences*, **74**, 229–248.

Baidu, M., Schwendike, J., Marsham, J. H. and Bain, C. (2022) Effects of vertical wind shear on intensities of mesoscale convective systems over West and Central Africa. *Atmospheric Science Letters*, **23**, e1094.

Best, M. J., Pryor, M., Clark, D. B., Rooney, G. G., Essery, R., Ménard, C. B., Edwards, J. M., Hendry, M. A., Porson, A., Gedney, N. et al. (2011) The Joint UK Land Environment Simulator (JULES), model description–Part 1: energy and water fluxes. *Geoscientific Model Development*, **4**, 677–699.

Bickle, M. E., Marsham, J. H., Griffiths, S. D., Ross, A. N. and Crook, J. (2022) The influence of the diurnal cycle in wind shear and thermodynamics on squall lines in the West African Monsoon. *Journal of the Atmospheric Sciences*, **79**, 2125–2143.

Bickle, M. E., Marsham, J. H., Ross, A. N., Rowell, D. P., Parker, D. J. and Taylor, C. M. (2021) Understanding mechanisms for trends in Sahelian squall lines: Roles of thermodynamics and shear. *Quarterly Journal of the Royal Meteorological Society*, **147**, 983–1006.

Birch, C. E., Marsham, J. H., Parker, D. J. and Taylor, C. M. (2014a) The scale dependence and structure of convergence fields preceding the initiation of deep convection. *Geophysical Research Letters*, **41**, 4769–4776.

Birch, C. E., Parker, D., Marsham, J., Copsey, D. and Garcia-Carreras, L. (2014b) A seamless assessment of the role of convection in the water cycle of the West African Monsoon. *Journal of Geophysical Research: Atmospheres*, **119**, 2890–2912.

Bony, S., Stevens, B., Frierson, D. M., Jakob, C., Kageyama, M., Pincus, R., Shepherd, T. G., Sherwood, S. C., Siebesma, A. P., Sobel, A. H. et al. (2015) Clouds, circulation and climate sensitivity. *Nature Geoscience*, **8**, 261–268.

Brown, A., Milton, S., Cullen, M., Golding, B., Mitchell, J. and Shelly, A. (2012) Unified modeling and prediction of weather and climate: A 25–year journey. *Bulletin of the American Meteorological Society*, **93**, 1865–1877.

Bryan, G. H., Knievel, J. C. and Parker, M. D. (2006) A multimodel assessment of RKW theory's relevance to squall-line characteristics. *Monthly weather review*, **134**, 2772–2792.

Bush, M., Boutle, I., Edwards, J., Finnenkoetter, A., Franklin, C., Hanley, K., Jayakumar, A., Lewis, H., Lock, A., Mittermaier, M. et al. (2023) The second Met Office Unified Model–JULES Regional Atmosphere and Land configuration, RAL2. *Geoscientific Model Development*, **16**, 1713–1734.

Bush, M., Flack, D. L. A., Lewis, H. W., Bohnenstengel, S. I., Short, C. J., Franklin, C., Lock, A. P., Best, M., Field, P., McCabe, A., Weverberg, K. V., Berthou, S., Boutle, I., Brooke, J. K., Cole, S., Cooper, S., Dow, G., Edwards, J., Finnenkoetter, A., Furtado, K., Halladay, K., Hanley, K., Hendry, M. A., Hill, A., Jayakumar, A., Jones, R. W., Lean, H., Lee, J. C. K., Malcolm, A., Mittermaier, M., Mohandas, S., Moore, S., Morcrette, C., North, R., Porson, A., Rennie, S., Roberts, N., Roux, B., Sanchez, C., Su, C.-H., Tucker, S., Vosper, S., Walters, D., Warner, J., Webster, S., Weeks, M., Wilkinson, J., Whitall, M., Williams, K. D. and Zhang, H. (2024) The third Met Office Unified Model–JULES Regional Atmosphere and Land Configuration, RAL3. *Submitted to Geoscientific Model Development*.

Chen, X., Leung, L. R., Feng, Z. and Yang, Q. (2023) Environmental Controls on MCS Lifetime Rainfall over Tropical Oceans. *Geophysical Research Letters*, **50**, e2023GL103267.

Clark, P., Browning, K., Forbes, R., Morcrette, C., Blyth, A. and Lean, H. (2014) The evolution of an MCS over southern England. Part 2: Model simulations and sensitivity to microphysics. *Quarterly Journal of the Royal Meteorological Society*, **140**, 458–479.

Crook, J., Klein, C., Folwell, S., Taylor, C. M., Parker, D. J., Stratton, R. and Stein, T. (2019) Assessment of the Representation of West African Storm Lifecycles in Convection-Permitting Simulations. *Earth and Space Science*, **6**, 818–835.

Crook, N. A. and Moncrieff, M. W. (1988) The effect of large-scale convergence on the generation and maintenance of deep moist convection. *Journal of the Atmospheric Sciences*, **45**, 3606–3624.

Dione, C., Lothon, M., Badiane, D., Campistron, B., Couvreux, F., Guichard, F. and Sall, S. (2014) Phenomenology of sahelian convection observed in niamey during the early monsoon. *Quarterly Journal of the Royal Meteorological Society*, **140**, 500–516.

Donahue, A. S., Caldwell, P. M., Bertagna, L., Beydoun, H., Bogenschutz, P. A., Bradley, A., Clevenger, T. C., Foucar, J. G., Golaz, J.-C., Guba, O. et al. (2024) To exascale and beyond–The Simple Cloud-Resolving E3SM Atmosphere Model (SCREAM), a performance portable global atmosphere model for cloud-resolving scales. *Journal of Advances in Modeling Earth Systems*, **16**, e2024MS004314.

Drager, A. J. and van den Heever, S. C. (2017) Characterizing convective cold pools. *Journal of Advances in Modeling Earth Systems*, **9**, 1091–1115.

Engerer, N. A., Stensrud, D. J. and Coniglio, M. C. (2008) Surface characteristics of observed cold pools. *Monthly Weather Review*, **136**, 4839–4849.

Feng, Z., Leung, L. R., Hardin, J., Terai, C. R., Song, F. and Caldwell, P. (2023) Mesoscale Convective Systems in DYAMOND Global Convection–Permitting Simulations. *Geophysical Research Letters*, **50**, e2022GL102603.

Feng, Z., Prein, A. F., Kukulies, J., Fiolleau, T., Jones, W. K., Maybee, B., Moon, Z., Ocasio, K. M. N., Dong, W., Molina, M. J. et al. (2024) Mesoscale Convective Systems tracking Method Intercomparison (MCSMIP): Application to DYAMOND Global km-scale Simulations. *Authorea Preprints*.

Field, P. R., Hill, A., Shipway, B., Furtado, K., Wilkinson, J., Miltenberger, A., Gordon, H., Grosvenor, D. P., Stevens, R. and Van Weverberg, K. (2023) Implementation of a double moment cloud microphysics scheme in the UK met office regional numerical weather prediction model. *Quarterly Journal of the Royal Meteorological Society*.

Fuglestvedt, H. F. and Haerter, J. O. (2020) Cold pools as conveyor belts of moisture. *Geophysical Research Letters*, **47**, e2020GL087319.

Garcia-Carreras, L., Marsham, J., Parker, D., Bain, C., Milton, S., Saci, A., Salah-Ferroudj, M., Ouchene, B. and Washington, R. (2013) The impact of convective cold pool outflows on model biases in the Sahara. *Geophysical Research Letters*, **40**, 1647–1652.

Garcia-Carreras, L., Marsham, J. H., Stratton, R. A. and Tucker, S. (2021) Capturing convection essential for projections of climate change in African dust emission. *npj Climate and Atmospheric Science*, **4**.

Grant, L. D., Lane, T. P. and van den Heever, S. C. (2018) The role of cold pools in tropical oceanic convective systems. *Journal of the Atmospheric Sciences*, **75**, 2615–2634.

Grant, L. D., Moncrieff, M. W., Lane, T. P. and van den Heever, S. C. (2020) Shear-parallel tropical convective systems: Importance of cold pools and wind shear. *Geophysical Research Letters*, **47**, e2020GL087720.

Hoeller, J., Haerter, J. O. and Da Silva, N. A. (2024) Characteristics of station-derived convective cold pools over equatorial Africa. *Geophysical Research Letters*, **51**, e2023GL107308.

Hohenegger, C., Korn, P., Linardakis, L., Redler, R., Schnur, R., Adamidis, P., Bao, J., Bastin, S., Behravesh, M., Bergemann, M. et al. (2023) ICON–Sapphire: simulating the components of the Earth system and their interactions at kilometer and subkilometer scales. *Geoscientific Model Development*, **16**, 779–811.

Houze Jr, R. A. (2004) Mesoscale convective systems. *Reviews of Geophysics*, **42**.

Hsiao, W.-T., Maloney, E. D., Leitmann-Niimi, N. M. and Kummerow, C. D. (2024) Observed relationships between sea surface temperature, vertical wind shear, tropical organized deep convection, and radiative effects. *Journal of Climate*, **37**, 1277–1293.

Jeevanjee, N. and Romps, D. M. (2013) Convective self-aggregation, cold pools, and domain size. *Geophysical Research Letters*, **40**, 994–998.

Jones, R. W., Sanchez, C., Lewis, H., Warner, J., Webster, S. and Macholl, J. (2023) Impact of domain size on tropical precipitation within explicit convection simulations. *Geophysical Research Letters*, **50**, e2023GL104672.

Khairoutdinov, M. and Randall, D. (2006) High-resolution simulation of shallow-to-deep convection transition over land. *Journal of the Atmospheric Sciences*, **63**, 3421–3436.

Klein, C., Jackson, L. S., Parker, D. J., Marsham, J. H., Taylor, C. M., Rowell, D. P., Guichard, F., Vischel, T., Famien, A. M. and Diedhiou, A. (2021) Combining CMIP data with a regional convection-permitting model and observations to project extreme rainfall under climate change. *Environmental Research Letters*, **16**, 104023.

Klein, C. and Taylor, C. M. (2020) Dry soils can intensify mesoscale convective systems. *Proceedings of the National Academy of Sciences*, **117**, 21132–21137.

Lane, T. P. and Zhang, F. (2011) Coupling between gravity waves and tropical convection at mesoscales. *Journal of the Atmospheric Sciences*, **68**, 2582–2598.

Liu, C. and Moncrieff, M. W. (2004) Effects of convectively generated gravity waves and rotation on the organization of convection. *Journal of the Atmospheric Sciences*, **61**, 2218–2227.

Mapes, B. E. (1993) Gregarious tropical convection. *Journal of the Atmospheric Sciences*, **50**, 2026–2037.

Mapes, B. E., Warner, T. T. and Xu, M. (2003) Diurnal patterns of rainfall in northwestern South America. Part III: Diurnal gravity waves and nocturnal convection offshore. *Monthly Weather Review*, **131**, 830–844.

Marsham, J. H., Dixon, N. S., Garcia-Carreras, L., Lister, G. M., Parker, D. J., Knippertz, P. and Birch, C. E. (2013) The role of moist convection in the West African monsoon system: Insights from continental–scale convection–permitting simulations. *Geophysical Research Letters*, **40**, 1843–1849.

Marsham, J. H., Knippertz, P., Dixon, N. S., Parker, D. J. and Lister, G. M. (2011) The importance of the representation of deep convection for modeled dust-generating winds over West Africa during summer. *Geophysical Research Letters*, **38**.

Mathon, V., Laurent, H. and Lebel, T. (2002) Mesoscale convective system rainfall in the sahel. *Journal of Applied Meteorology and Climatology*, **41**, 1081–1092.

Maurer, V., Bischoff-Gauß, I., Kalthoff, N., Gantner, L., Roca, R. and Panitz, H.-J. (2017) Initiation of deep convection in the Sahel in a convection-permitting climate simulation for northern Africa. *Quarterly Journal of the Royal Meteorological Society*, **143**, 806–816.

Maybee, B., Marsham, J., Klein, C., Parker, D. J., Barton, E. J., Taylor, C. M., Lewis, H., Sanchez, C., Jones, R. W. and Warner, J. L. (2024) Wind shear effects in convection–permitting models influence mcs rainfall and forcing of tropical circulation. *Geophysical Research Letters*, **51**.

Meyer, B. and Haerter, J. O. (2020) Mechanical forcing of convection by cold pools: Collisions and energy scaling. *Journal of Advances in Modeling Earth Systems*, **12**, e2020MS002281.

Miao, J.-E. and Yang, M.-J. (2020) A modeling study of the severe afternoon thunderstorm event at Taipei on 14 June 2015: The roles of sea breeze, microphysics, and terrain. *Journal of the Meteorological Society of Japan. Ser. II*, **98**, 129–152.

Moncrieff, M. W. (1992) Organized convective systems: Archetypal dynamical models, mass and momentum flux theory, and parametrization. *Quarterly Journal of the Royal Meteorological Society*, **118**, 819–850.

Mulholland, J. P., Peters, J. M. and Morrison, H. (2021) How does vertical wind shear influence entrainment in squall lines? *Journal of the Atmospheric Sciences*, **78**, 1931–1946.

Pandya, R. E. and Durran, D. R. (1996) The influence of convectively generated thermal forcing on the mesoscale circulation around squall lines. *Journal of the Atmospheric Sciences*, **53**, 2924–2951.

Parker, D. J. and Diop-Kane, M. (2017) *Meteorology of tropical West Africa: The forecasters' handbook*. John Wiley & Sons.

Prein, A. F., Liu, C., Ikeda, K., Trier, S. B., Rasmussen, R. M., Holland, G. J. and Clark, M. P. (2017) Increased rainfall volume from future convective storms in the US. *Nature Climate Change*, **7**, 880–884.

Prein, A. F., Rasmussen, R. M., Wang, D. and Giangrande, S. E. (2021) Sensitivity of organized convective storms to model grid spacing in current and future climates. *Philosophical Transactions of the Royal Society A*, **379**, 20190546.

Provod, M., Marsham, J., Parker, D. and Birch, C. (2016) A characterization of cold pools in the West African Sahel. *Monthly Weather Review*, **144**, 1923–1934.

Rackow, T., Pedruzo-Bagazgoitia, X., Becker, T., Milinski, S., Sandu, I., Aguridan, R., Bechtold, P., Beyer, S., Bidlot, J., Boussetta, S. et al. (2024) Multi-year simulations at kilometre scale with the Integrated Forecasting System coupled to FESOM2. 5/NEMOv3. 4. *EGUsphere*, **2024**, 1–59.

Robe, F. R. and Emanuel, K. A. (2001) The effect of vertical wind shear on radiative–convective equilibrium states. *Journal of the Atmospheric Sciences*, **58**, 1427–1445.

Rotunno, R., Klemp, J. B. and Weisman, M. L. (1988) A theory for strong, long-lived squall lines. *Journal of Atmospheric Sciences*, **45**, 463–485.

Schumacher, R. S. (2009) Mechanisms for quasi-stationary behavior in simulated heavy-rain-producing convective systems. *Journal of the Atmospheric Sciences*, **66**, 1543–1568.

Senior, C. A., Marsham, J. H., Berthou, S., Burgin, L. E., Folwell, S. S., Kendon, E. J., Klein, C. M., Jones, R. G., Mittal, N., Rowell, D. P. et al. (2021) Convection permitting regional climate change simulations for understanding future climate and informing decision making in Africa. *Bulletin of the American Meteorological Society*, 1–46.

Slingo, J., Bates, P., Bauer, P., Belcher, S., Palmer, T., Stephens, G., Stevens, B., Stocker, T. and Teutsch, G. (2022) Ambitious partnership needed for reliable climate prediction. *Nature Climate Change*, **12**, 499–503.

Stein, T. H., Hogan, R. J., Hanley, K. E., Nicol, J. C., Lean, H. W., Plant, R. S., Clark, P. A. and Halliwell, C. E. (2014) The three-dimensional morphology of simulated and observed convective storms over southern England. *Monthly Weather Review*, **142**, 3264–3283.

Stoelinga, M. T., Locatelli, J. D., Schwartz, R. D. and Hobbs, P. V. (2003) Is a cold pool necessary for the maintenance of a squall line produced by a cold front aloft? *Monthly weather review*, **131**, 95–115.

Taylor, C. M., Belušić, D., Guichard, F., Parker, D. J., Vischel, T., Bock, O., Harris, P. P., Janicot, S., Klein, C. and Panthou, G. (2017) Frequency of extreme Sahelian storms tripled since 1982 in satellite observations. *Nature*, **544**, 475–478.

Taylor, C. M., Gounou, A., Guichard, F., Harris, P. P., Ellis, R. J., Couvreux, F. and De Kauwe, M. (2011) Frequency of Sahelian storm initiation enhanced over mesoscale soil-moisture patterns. *Nature Geoscience*, **4**, 430–433.

Thorpe, A., Miller, M. and Moncrieff, M. (1982) Two–dimensional convection in non–constant shear: A model of mid–latitude squall lines. *Quarterly Journal of the Royal Meteorological Society*, **108**, 739–762.

Tomassini, L., Willett, M., Sellar, A., Lock, A., Walters, D., Whitall, M., Sanchez, C., Heming, J., Earnshaw, P., Rodriguez, J. M. et al. (2023) Confronting the convective gray zone in the global configuration of the Met Office Unified Model. *Journal of Advances in Modeling Earth Systems*, **15**, e2022MS003418.

Tompkins, A. M. (2001) Organization of tropical convection in low vertical wind shears: The role of cold pools. *Journal of the Atmospheric Sciences*, **58**, 1650–1672.

Torri, G., Kuang, Z. and Tian, Y. (2015) Mechanisms for convection triggering by cold pools. *Geophysical Research Letters*, **42**, 1943–1950.

Trier, S. B., Marsham, J. H., Davis, C. A. and Ahijevych, D. A. (2011) Numerical simulations of the postsunrise reorganization of a nocturnal mesoscale convective system during 13 June IHOP_2002. *Journal of the Atmospheric Sciences*, **68**, 2988–3011.

Trzeciak, T. M., Garcia-Carreras, L. and Marsham, J. H. (2017) Cross-Saharan transport of water vapor via recycled cold pool outflows from moist convection. *Geophysical Research Letters*, **44**, 1554–1563.

Tulich, S. N. and Kiladis, G. N. (2012) Squall lines and convectively coupled gravity waves in the tropics: why do most cloud systems propagate westward? *Journal of the Atmospheric Sciences*, **69**, 2995–3012.

Tulich, S. N. and Mapes, B. E. (2008) Multiscale convective wave disturbances in the tropics: Insights from a two-dimensional cloud-resolving model. *Journal of the Atmospheric Sciences*, **65**, 140–155.

Van Weverberg, K., Morcrette, C. J., Boutle, I., Furtado, K. and Field, P. R. (2021) A bimodal diagnostic cloud fraction parameterization. Part I: Motivating analysis and scheme description. *Monthly Weather Review*, **149**, 841–857.

Vizy, E. K. and Cook, K. H. (2018) Mesoscale convective systems and nocturnal rainfall over the West African Sahel: role of the Inter-tropical front. *Climate Dynamics*, **50**, 587–614.

Weisman, M. L. and Rotunno, R. (2004) "a theory for strong long-lived squall lines" revisited. *Journal of the Atmospheric Sciences*, **61**, 361–382.

Yang, G.-Y. and Slingo, J. (2001) The Diurnal Cycle in the Tropics. *Monthly Weather Review*, **129**, 784–801.

Yang, M.-J. and Houze, R. A. (1996) Momentum budget of a squall line with trailing stratiform precipitation: Calculations with a high-resolution numerical model. *Journal of the Atmospheric Sciences*, **53**, 3629–3652.

Zhao, S., Cook, K. H. and Vizy, E. K. (2024) Greenhouse gas-induced modification of intense storms over the west african sahel through thermodynamic and dynamic processes. *Climate Dynamics*, 1–26.

GRAPHICAL ABSTRACT

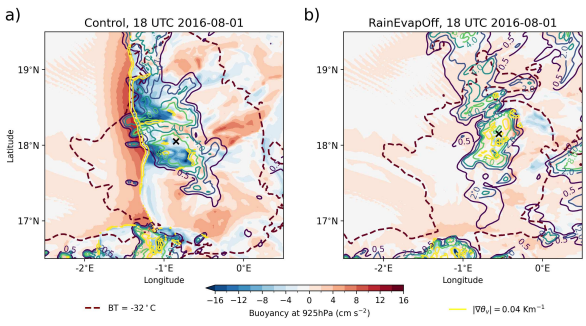

Cold pools are a ubiquitous feature of MCSs with important upscale impacts on West African climate, but their role in the maintenance of tropical MCSs remains debated. Using a 40 day model with explicit convection and no rainfall evaporation, we show that cold pools do not play a primary role in Sahel MCS development or maintenance. Moreover, we find that the positive feedback of wind shear on convective intensity is not sensitive to cold pool suppression.